ACS OMEGA

http://pubs.acs.org/journal/acsodf

Article

Potassium Silicate as Low-Temperature Binder in 3D-Printed Porous Structures for CO_2 Separation

Ben Sutens,* Yoran De Vos, Brieuc Verougstraete, Joeri F. M. Denayer, and Marleen Rombouts

Cite This: *ACS Omega* 2023, 8, 4116−4126

Read Online

ACCESS | Metrics & More | Article Recommendations | Supporting Information

ABSTRACT: Activated carbon sorbents were directly 3D-printed into highly adaptable monolithic/multi-channel systems by using potassium silicate as a low-temperature binder. By employing emerging 3D-printing technologies, monolithic structured sorbents were printed and fully characterized using N_2, Ar, and CO_2-sorption and Hg-intrusion porosimetry. The CO_2-capture performance and the required temperature for active-site regeneration were evaluated by thermogravimetric analysis-looping experiments. A mechanically stable activated carbon sorbent was developed with an increased carbon capture performance, even when a room-temperature regeneration by N_2 purging was applied. Although the CO_2 uptake slightly dropped after several cycles due to incomplete recovery at room temperature, a capacity increase of 25% was observed in comparison with the original activated carbon powder. To improve the recovery of the active sorbent, an optimization of the desorption step was performed by increasing the regeneration temperature up to 150 °C. This resulted in a CO_2 uptake of the composite material of 0.76 mmol/g, almost tripling the working capacity of the original activated carbon powder (0.28 mmol/g). An in situ X-ray diffraction study was carried out to confirm the proposed sorption mechanism, indicating the presence of potassium bicarbonates and confirming the combination of physisorption and chemisorption in our composites. Finally, the structured adsorbent was heated homogeneously by applying a current through the monolith. These results describe the development of a new type of 3D-printed regenerable CO_2 sorbents by using potassium silicate as a low-temperature binder, providing high mechanical strength, good chemical and thermal stability, and improving the total CO_2 capacity. Moreover, the developed monolith is showing a homogeneous resistivity, leading to uniform Joule heating of the CO_2 adsorbent.

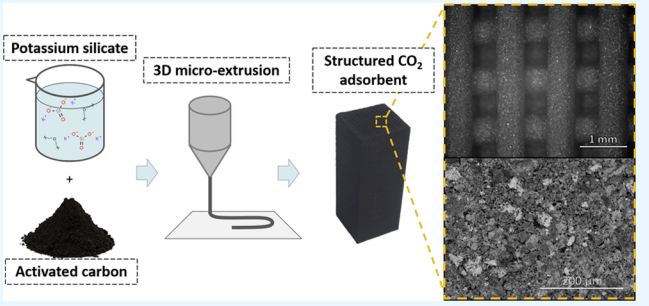

INTRODUCTION

The emission of greenhouse gases into the atmosphere, especially carbon dioxide, is a worldwide acknowledged problem. Throughout the last years, a significant increase in CO_2 emission has been observed which is predominantly caused by human activities including industry, transportation, and the use of fossil fuels as an energy source. Since CO_2 emission continues to steadily increase every year, it is considered as the primary driver of climate change and one of the most pressing challenges. Therefore, more and more research has been dedicated in the last years to develop innovative processes to reduce the ecological impact of CO_2 by capturing it preventively as well as using it as a building block for fuels, polymers, and other valuable chemicals, also known as carbon capture, utilization, and storage.

Nowadays, most commercial CO_2 capture processes involve the use of liquid amine solutions. However, these amines are plagued by several drawbacks including high energy consumption during regeneration, thermal and oxidative solvent degradation, and evaporation, as well as formation of corrosion products.[1−3] Therefore, the interest has shifted to alternative CO_2 separation processes, including thermal swing adsorption (TSA) using solid porous materials which show a high selectivity for CO_2 while reducing the energy consumption and amount of waste water significantly.[4] Raganati et al. described the use of fine porous activated carbon in a laboratory-scale TSA fluidized-bed setup obtaining a high recovery rate as well as a high purity CO_2 stream.[5] Ben-Mansour et al. evaluated the performance improvement by computational fluid dynamics (CFD) modeling for the use of Mg-MOF74 in a TSA process, showing an improvement in productivity and overall power consumption.[6] Rainone et al. showed the promising potential of activated carbon and carbon molecular sieves (CMS) adsorbents at a low regeneration temperature for biogas upgrading.[7] Morales-Ospino et al. evaluated the energy efficiency of two TSA configurations using a commercial 13X zeolite at moderate desorption temperatures.[8]

Received: November 2, 2022
Accepted: December 22, 2022
Published: January 18, 2023

Although this method seems very promising, conventional TSA processes often show long cycle times due to the indirect heating of the adsorbent. Consequently, electrical swing adsorption (ESA) by the use of Joule heating has shown to be a promising alternative. On contrary to the conventional TSA processes, the adsorbent is directly heated by an electric current throughout the adsorbent which reduces the total cycle time and enhances the overall efficiency significantly.[9−11] Moreover, the system is not contaminated with water unlike TSA processes where steam regeneration is often used.

Conventional sorbent shapes include packings of beads, pellets, and extrudates, but have limitations in terms of pressure drops, inefficient use of active material at short contact times, and increased attrition. Therefore, structured adsorbents including monolithic structures show great potential due to a uniform flow pattern, resulting in low pressure drop and improved heat- and mass transfer.[12−14] Moreover, structured adsorbents enable the formation of a homogeneous electrical conduction and heating during an ESA process, avoiding the development of hot spots.

One way to develop monolithic-shaped adsorbents includes the washcoating of extruded inert supports. However, this often leads to a limited sorbent loading per unit volume and poor surface adhesion. Contrary to coating of a monolithic inert support, additive manufacturing or direct 3D-printing of the sorbent material into a monolithic shape has proven its potential and enables the development of an optimal porous structure with a specific design, tailored to the application while showing a high sorbent loading per volume material.[15,16]

Common adsorbent materials typically involve porous materials due to their high specific surface area and high adsorption capacities. Two categories can be distinguished, based on their adsorption process: (I) activated carbon,[17,18] zeolites,[12,19] and porous polymers,[20,21] metal organic frameworks (MOFs),[22,23] and covalent organic frameworks (COFs),[24,25] in which adsorption occurs mainly due to physisorption and (II) metal-based adsorbents (e.g., Na_2CO_3, K_2CO_3, CaO, ...)[26,27] and hybrid organic/inorganic sorbents including amine-functionalized polymers or inert supports,[28,29] in which adsorption occurs due to chemisorption. Metal-based adsorbents and specifically carbonates provide several advantages that make them desirable for carbon capture, including their inexpensiveness, nonvolatility, resistance to degradation, and low binding energy with CO_2 enabling an energy-efficient capture process. A promising combination includes the impregnation of potassium carbonate onto various supports including activated carbon, presenting high CO_2 capture capacity and reaction rate at fairly low temperatures due to the microscopic architecture of the activated carbon powder.[30−32] However, most sorbents that have been reported were evaluated in powder or pelletized form. Shaping of these adsorbents by 3D-printing and specifically 3D micro-extrusion typically includes the addition of a combination of inorganic binders and organic binders, which can function as a rheology modifier and provide green strength. Thakkar et al. and Lawson et al. both describe the use of a combination of bentonite clay and poly(vinyl alcohol) (PVA) for the development of 3D-printed MOF and carbon monoliths for CO_2 adsorption, respectively.[33,34] Couck et al. developed a SAPO-34 monolith for gas separation using a methylcellulose solution.[35] Lefevere et al. described a binder recipe of a combination of methylcellulose and bentonite for the development of a 3D-printed ZIF-8 adsorbent.[16] Regufe et al. incorporated a carboxymethylcellulose solution to provide green strength to an electrically conductive zeolite/activated carbon monolith.[17]

Typically, the use of these binders requires a high-temperature thermal treatment in order to remove the organics and obtain a stable, strong, and accessible porous structured material. This typically leads to a loss in specific surface area, porosity, and consequently in CO_2 sorption capacity.[15,17] In order to avoid these challenges, a low-temperature binder which adsorbs CO_2 and contributes to the total sorption capacity could offer a possible solution and could result in the retainment of the total capacity.

In our recent study on biogas upgrading by a 3D-printed activated carbon monolith through electrical swing adsorption, the influence of the electrification conditions (e.g., voltage, electrification time, and purge conditions) on the heating, regeneration efficiency, and resulting purity was extensively investigated.[36] Although sorbents with better CO_2-selectivity are required for potential use of ESA in biogas upgrading, the monolith used for the ESA experiments showed a homogeneous temperature distribution during Joule heating and excellent mechanical and thermal stability.[36] While the earlier publication was focused on the ESA performance and the impact of process conditions on practical applicability in biogas upgrading, the 3D-printing formulation optimization and impact of the sorbent composition on the CO_2-adsorption performance have not been discussed.

Therefore, this paper focuses on the development of the formulation and the characterization of the 3D-printed activated carbon adsorbents, more specifically on the role of the commercial silicate binder. A commercial potassium silicate solution was combined with activated carbon and subsequently shaped by 3D micro-extrusion, resulting in a structured hybrid adsorbent. The use of a silicate binder resulted in a high mechanical strength without the need of a high-temperature thermal treatment, good chemical and thermal stability while retaining or even improving the total CO_2 capacity. Several publications describe the use of lithium or sodium metasilicate as CO_2 sorbents in powder or pelletized form.[37−41] However, the use of potassium silicate as a binder for 3D-printed structures offers an innovative technique to hierarchically structure CO_2 sorbents. Through extensive characterization of the printed monoliths, the role of the silicate binder and the CO_2-adsorption mechanism have been elucidated. Finally, Joule heating experiments were performed with improved thermal imaging, showcasing the homogeneous temperature distribution and fast cycling possibilities of the hybrid material.

EXPERIMENTAL SECTION

Paste Preparation and Monolith Printing. The 3D-printing paste was prepared by a mixture of activated carbon powder (Norit SX1G, Cabot Corporation), a commercial silicate glue (Graphi-bond 669T, Aremco Products), and distilled water. Prior to mixing, the activated carbon was sieved through a 45 μm mesh, resulting in a particle size distribution with a D50 value of 21.86 μm. Using an ARE Thinky mixer, the different components were mixed in several ratios to obtain a printable paste, while providing high mechanical strength and a maximized total CO_2 capacity. Subsequently, the paste was loaded into a syringe and extruded by using a mechanically driven piston, mounted on a computer numerically controlled (CNC) x-y-z stage. A constant volume flow was ensured by the piston, extruding fibers through a nozzle of 600 μm. Squared

https://doi.org/10.1021/acsomega.2c07074
ACS Omega 2023, 8, 4116−4126

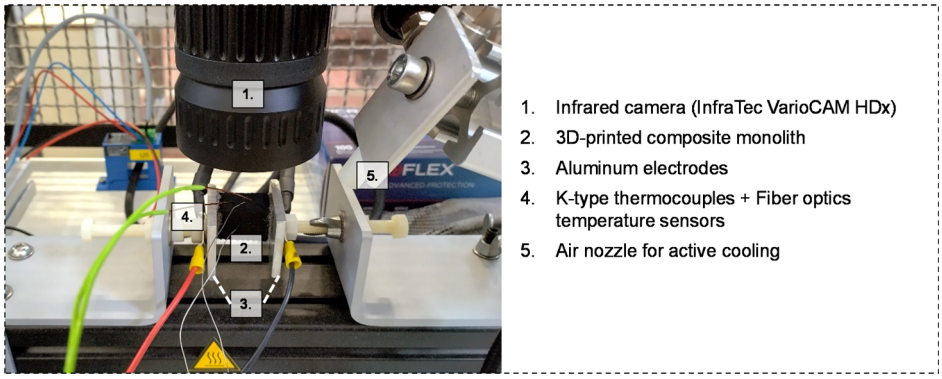

Figure 1. Overview of the in-house built setup which was used for cyclic Joule heating experiments of the structured composite adsorbent.

monolithic-type structures were constructed layer-by-layer until a beam of 5 cm height and 2 cm width was obtained. The programmed scan spacing between neighboring fibers was kept at 1200 μm while each successive layer was rotated with 90°. After printing, the structures were dried using a Thermo Scientific Heratherm at 94 °C for 8 h to obtain a mechanically strong printed monolith. No additional high-temperature thermal treatment was performed. The linear shrinkage was also analyzed based on the length and width before and after the drying process.

Adsorbent Characterization. Characterization of the glue was performed by means of Fourier transform−infrared spectroscopy using a Thermo Scientific Nicolet NEXUS spectrophotometer and inductively coupled plasma (ICP) spectroscopy using an Agilent Technologies 5100 ICP-OES. Specific surface area and micropore volume determination of the AC powder and 3D-printed adsorbent were analyzed from N_2 isotherms at liquid nitrogen temperatures (77 K) on a Quantachrome Autosorb-iQ−MP (volumetric). Sample activation was performed overnight at 200 °C under vacuum. A CO_2 isotherm at 273.15 K and Ar at 87 K were measured using a Quantachrome Autosorb-1 to gain insights into the (ultra)micro- and mesopore distribution. The CO_2 isotherm was analyzed using quenched solid density functional theory while the Ar isotherm was treated according to nonlocal density functional theory. Mercury intrusion porosimetry was performed on a Thermo electron Corporation Pascal 140−240 series. The pore size distribution was calculated using a contact angle of 140° and a surface tension of 480 Dynes/cm. He pycnometry was determined on a Micromeritics AccuPyc II. X-ray diffraction (XRD) measurements were carried out using a PANalytical X'Pert Pro Powder diffractometer operating with a Cu anode (CuKα; λ = 1.5405 Å) operated at a 40 kV voltage and 30 mA current. Phase identification was carried out using X'Pert PANalytical High Score Plus software. Scanning electron microscopy (SEM) with energy dispersive X-ray analysis (EDX) was performed by a FEI Nova NanoSEM 450. The mechanical strength of the 3D-printed adsorbent was analyzed using a compression strength test (top−bottom) with a compression speed of 0.5 mm/min.

The CO_2 capacity of the composite sorbent was analyzed using thermogravimetric analysis (TGA), performed on a NETZSCH STA449 F3 Jupiter. The composite sorbent was measured in crushed form with a typical sample mass of 100 mg to exclude any mass diffusion limitations. A looping sequence was programmed, consisting of three cycles in which CO_2 adsorption at 25 °C or elevated temperatures was induced for 3 h by a mixed flow of 9.1% CO_2 (10 mL/min) in N_2 (100 mL/min), followed by a desorption step of 3 h in which purely N_2 was used at RT or elevated temperatures, depending on the performed experiment. Prior to the first cycle, a regeneration step was performed for 3 h at 120 °C in order to activate the adsorbent by removing the physisorbed gases. As a reference, the same looping sequence was used to evaluate the impact of the shaping process by analyzing the CO_2 capacity of the structured monolith.

Joule Heating. The electrical resistivity was measured on the activated carbon powder as well as fibers of the composite using a two-probe method, using a Tektronix DMM4050 voltmeter and a power supply. Cyclic Joule heating experiments were performed using the structured composite sorbent on an in-house built system (Figure 1). The structured monolith was installed in between two aluminum plates, serving as the electrodes. To ensure an optimal electrode-monolith contact which is necessary for homogeneously heating of the monolith, the two parts were secured using butterfly screws. The contact between the two electrodes and the monolith was improved by using fine steel wool between the electrodes and the monolith. The aluminum plates were connected to a power supply (Statron 3256.1 Bench PSU), that allowed the application of a constant electric potential (0−36 V DC) or current (0−13 A). In the application test, a fixed current of 2.4 A was used to heat up the monolithic adsorbent, leading to a potential difference varying between 5.3 and 4.6 V at room temperature and maximum temperature, respectively. The power supply was turned on/off based on the measured temperature at the surface of the monolithic composite adsorbent using two K-type thermocouples connected with a GRAPHTEC GL240 data-logger. A cyclic experiment was executed by applying a fixed current of 2.4 A through the monolith, resulting in the heating of the material by Joule heating. When the temperature of the material reached the target set point of 90 °C, the current to the power supply was cut off. At the same time, a cooling nozzle located to the side of the monolithic adsorbent was activated, blowing approximately 10 SLPM of pressurized air on the structured monolith to induce active cooling of the sample. When the thermocouple detected a temperature below 19.8 °C, the power supply was activated again to apply the fixed current of 2.4 A through the composite monolith and initiating the second cycle.

During the cyclic experiments, the temperature of the monolith surface was monitored using an infrared camera (InfraTec VarioCAM HDx head 600 S) with a macro-lens (VarioCAM HDx 20 mm) combined with a close-up lens

https://doi.org/10.1021/acsomega.2c07074
ACS Omega 2023, 8, 4116−4126

(0.35×), leading to a pixel size of approximately 49 μm. The monitored surface temperature was also measured and corrected by two fiber optic temperature sensors (Rugged Monitoring L201) located in the field of view of the infrared camera.

RESULTS AND DISCUSSION

Characterization of Silicate Glue. Figure 2 shows the Fourier-transform infrared spectroscopy (FT-IR) spectrum of

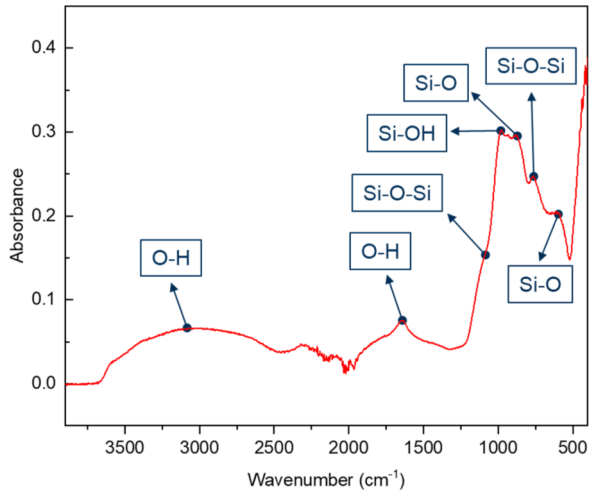

Figure 2. FT-IR spectrum of the silicate glue, measured in crushed powder form.

the pure silicate glue, which was dried at 94 °C overnight prior to crushing of the sample to perform the analysis. The silicate glue presented several characteristic vibration bands between 500 and 1100 cm^{-1}, confirming the nature of the binder. The presence of silicate and silica functionalities is acknowledged by the vibration bands detected at 609, 760, 877, 975, and 1100 cm^{-1} corresponding to the Si−O, Si−O−Si, Si−O, Si−OH, and Si−O−Si vibration, respectively. Moreover, a broad band between 3000 and 3500 cm^{-1} and a peak at 1638 cm^{-1} are observed, confirming the presence of hydroxyl functionalities and/or adsorbed water molecules at the silicate surface.

Additionally, ICP spectroscopy was performed to analyze the nature of the silicate glue in terms of counterions, which largely influences the total CO_2 capacity, the kinetic behavior, as well as regeneration temperature. ICP confirmed the presence of a mixture of potassium and sodium counterions, with potassium as the dominant species in a concentration of 74.7 g/L in comparison with sodium at 0.43 g/L. The concentration of silicon in the glue solution was equal to 129 g/L, resulting in a total Si/K + Na weight ratio of 1.72.

Additive Manufacturing of Monolithic Adsorbents. In the next step, the silicate glue was combined with an activated carbon powder in different proportions to develop a suitable paste composition for 3D-printing. The activated carbon/glue ratio varied between 70/30 and 40/60 to evaluate and balance the printability, mechanical strength of the sorbent after printing as well as after curing, and the impact of the used binder on the CO_2-sorption capacity. The CO_2 sorption capacity was measured using TGA by applying several cycles of a flow consisting of 9.1% CO_2 in N_2, as described in the Experimental Section.

As observed in Figure 3, a large improvement in CO_2 capacity is observed when adding increased amounts of glue

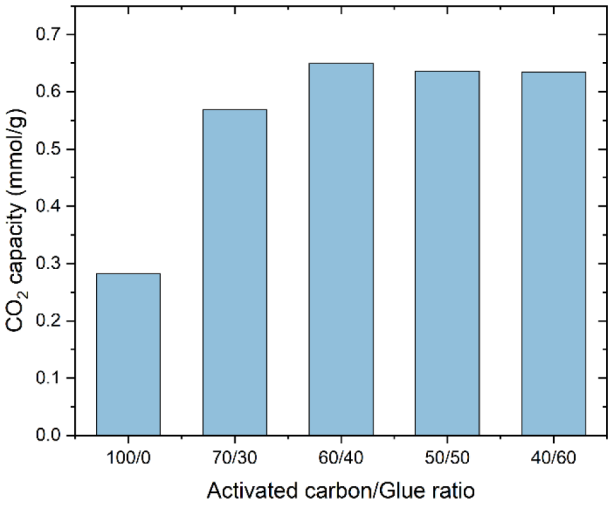

Figure 3. Effect of activated carbon/glue ratio on the total CO_2 capacity at 25 °C, analyzed by TGA (9.1% CO_2 in N_2 at 1 bar). The depicted CO_2 capacity is the gas uptake after a regeneration step of 3 h at 120 °C (first cycle).

to the activated carbon material, confirming the active contribution of the silicate glue. At a 70/30 ratio between activated carbon and glue, the CO_2-capacity at 25 °C doubles from 0.28 mmol/g for the activated carbon powder to 0.57 mmol/g for the composite. The mechanical strength at this composition is, however, insufficient to self-support a printed structure, and more glue is needed to achieve the necessary mechanical strength. Decreasing the ratio to 60/40 and 50/50 improved the mechanical strength, but a further decrease to 40/60 resulted in a collapse of the structure after printing due to the influence of the aqueous glue solution on the viscosity of the printing paste. Ratios higher than 50/50 are therefore unsuitable for 3D-printing as they resulted in phase separation and as the self-supportability of the printed monoliths was insufficient. While both 50/50 and 60/40 ratios yielded structures with similar CO_2-capture capacity, the choice between the two formulations was made based on the final mechanical strength and the printability of the developed composite paste. The 50/50 ratio, selected for scale-up, further characterization, and Joule heating tests displayed a CO_2 capture capacity of 0.62 mmol/g during the first cycle, after a degassing period of 3 h at 120 °C.

To take into account the effect of the glue on the density and volumetric capacity of the composite material, the density of the cured and dried glue, the pure activated carbon powder, and the selected 50/50 composite (cured and dried) was determined by He-pycnometry. The respective skeletal densities are 2.019 g/cm^3 (glue), 1.869 g/cm^3 (AC powder), and 1.817 g/cm^3 (composite). These results indicate a very minor decrease in skeletal density when combining the glue with the activated carbon powder, resulting in the observation of a similar trend in terms of the volumetric capacity of the composite material compared to the CO_2-capacity based on weight (activated carbon powder 0.52 vs 1.14 mmol/cm^3 for the printed AC-silicate composite). These results indicate that the silicate glue binder has a tremendous effect on the capture capacity of the printed monolithic adsorbents.

https://doi.org/10.1021/acsomega.2c07074
ACS Omega 2023, 8, 4116−4126

The optimized paste formulation was subsequently loaded into a syringe and 3D-printed into monolithic-type structures using a 600 μm nozzle. The printed monoliths were then transferred to the drying furnace at 94 °C for at least 8 h to achieve mechanically strong sorbent monoliths (>1 MPa, Figure S1 in Supporting Information). During the low-temperature treatment, a limited linear shrinkage based on the dimensions before and after drying of up to 10% was observed without distortion. The final monoliths are depicted in Figure 4.

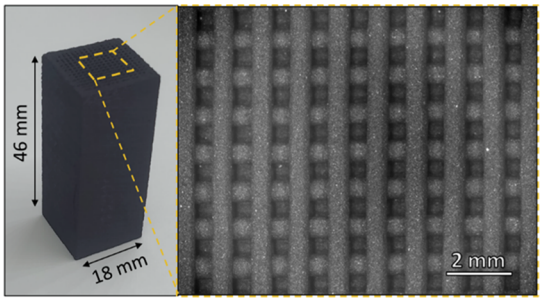

Figure 4. Images of the 3D-printed activated carbon/silicate glue composite, accompanied by an optical microscopy image to determine the fiber diameter and interfilament spacing. After drying, the final monoliths consist of fibers with a diameter of ~580 μm and an interfilament spacing of ~600 μm.

Adsorbent Characterization. Scanning electron microscopy images of a single composite fiber were taken to evaluate the distribution of the silicate glue. A highly porous fiber was observed, while the silicate glue was homogeneously distributed throughout the fiber, as shown in Figure 5 and

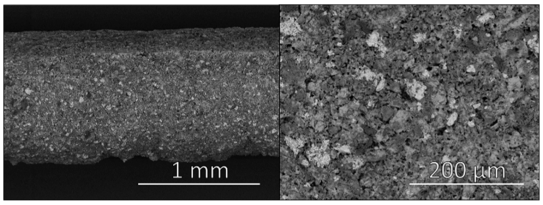

Figure 5. SEM images of a single extruded fiber consisting of the activated carbon powder and silicate glue.

on the EDX spectra presented in the Supporting Information (Figure S2). This provides an indication of an excellent wetting of the activated carbon powder (black platelets) by the glue, further confirmed by the minor decrease in density of the composite material versus the original activated carbon powder and cured glue.

A complete porosity characterization was performed using a combination of several techniques, including N_2, Ar, and CO_2 sorption as well as mercury intrusion porosimetry.

N_2 isotherms at 77 K of the crushed monolith structure in comparison with the activated carbon powder are shown in Figure 6. A significant change in the isotherm shape is observed, indicating a clear difference in pore shape, size and total pore volume. The activated carbon powder shows a typical type IV isotherm with a hysteresis loop associated with capillary condensation, indicative of the presence of mesopores. This can be associated with the plate-like carbon particles, forming slit-like pores. Moreover, a steep increase is observed at the lower pressure range, indicating a significant

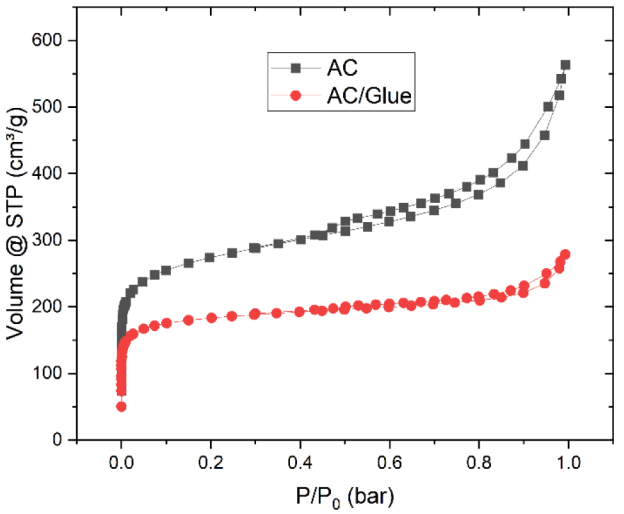

Figure 6. N_2 isotherms at 77 K of the activated carbon powder and the activated carbon/silicate glue composite.

amount of micropores as well. Addition of the silicate glue to the monolith structure clearly reduces the total meso- and microporosity, indicated by the disappearance of the hysteresis loop as well as the reduced uptake in the lower pressure range. A reduction of the Brunauer–Emmett–Teller (BET) value from 1010 m^2/g for the activated carbon powder to 700 m^2/g for the composite is observed. Using the *t*-plot method, a decrease of ~20% in micropore volume is obtained, due to the presence of the silicate glue. The cured glue itself displayed a very low BET surface area (1.2 m^2/g); therefore, a full isotherm of this material is not included.

This decrease in microporosity was also observed when using CO_2 and Ar adsorption isotherms to evaluate the microporous region. The use of Ar and CO_2 allows us to evaluate the (ultra-)micropore region more accurate in comparison with nitrogen, due to the absence of a quadrupole moment and the decreased reactivity.[42] Figure 7 shows the pore size distribution of both the activated carbon/silicate composite and activated carbon powder, as derived from the CO_2 isotherm at 273.15 K and the Ar isotherm at 87 K. The AC powder displays a large amount of micropores below 0.8 nm (0.24 cm^3/g) with a significant fraction at around 0.5–0.6 nm (>0.13 cm^3/g), which lead to the large uptake at low partial pressures. The composite material on the other hand shows a clear reduction in microporosity (<0.03 cm^3/g) below 0.8 nm, possibly due to the blockage of these micropores by the silicate binder. In the Ar porosimetry measurements, a significant reduction in total pore volume is shown for pores with a diameter larger than 1.0 nm. This clear decrease in microporosity is possibly induced by the "dilution" of the activated carbon due to the large presence of the silicate binder, responsible for 50% of the composite. An overview of the results using the different characterization techniques is shown in Table 1.

Figure 8 includes the pore size distribution measured by mercury intrusion porosimetry on the structured monolithic composite sorbent. Around 0.43 g of 3D-printed material was used to evaluate the macroporosity of the printed material. The measurement indicates a high amount of porosity (45.7%) inside the fibers. A total cumulative volume of 480 mm^3/g is shown, while the average pore radius and density were equal to 0.92 μm and 1.76 g/cm^3, respectively.

https://doi.org/10.1021/acsomega.2c07074
ACS Omega 2023, 8, 4116–4126

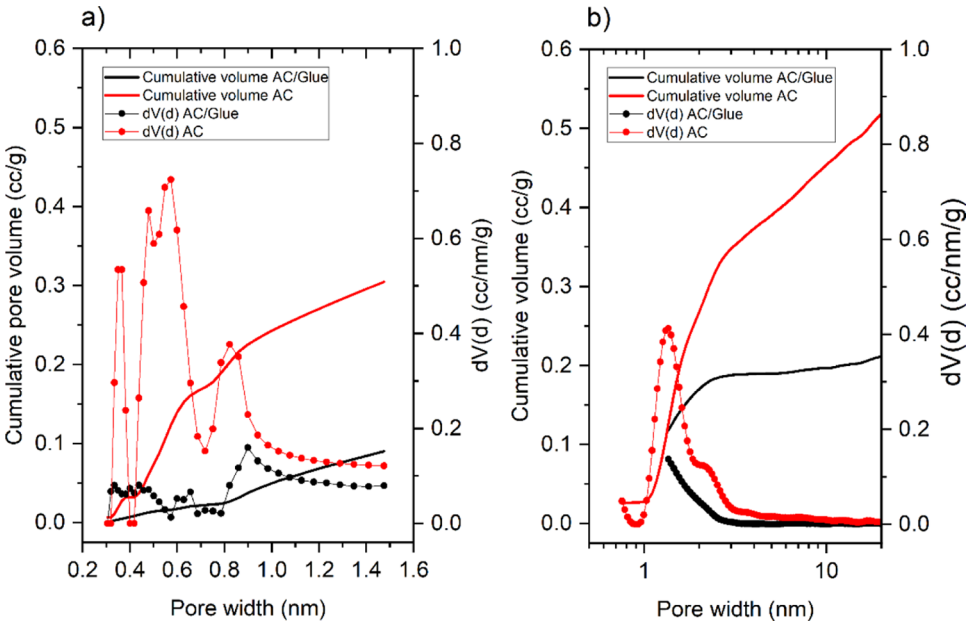

Figure 7. Pore size distributions of the activated carbon/silicate glue composite and activated carbon powder analyzed by (a) CO_2 porosimetry at 273.15 K and (b) Ar porosimetry at 87 K.

Table 1. Overview of the Porosity Properties of the Activated Carbon Powder Compared to the Activated Carbon/Silicate Composite

				activated carbon	activated carbon/glue
N_2	surface area	S_{BET}	[m^2/g]	1010	700
		S_{mic}	[m^2/g]	768	620
	pore volume	V_{tot}	[cm^2/g]	0.802	0.400
		V_{mic}	[cm^2/g]	0.327	0.252
Ar	surface area	S_{DFT}	[m^2/g]	1078	690
		S_{mic}	[m^2/g]	853	630
	pore volume	V_{tot}	[cm^2/g]	0.555	0.343
		V_{mic}	[cm^2/g]	0.274	0.172
CO_2	surface area	$S_{DFT(<1.5\ nm)}$	[m^2/g]	960	225
	pore volume	$V_{tot(<1.5\ nm)}$	[cm^2/g]	0.305	0.090

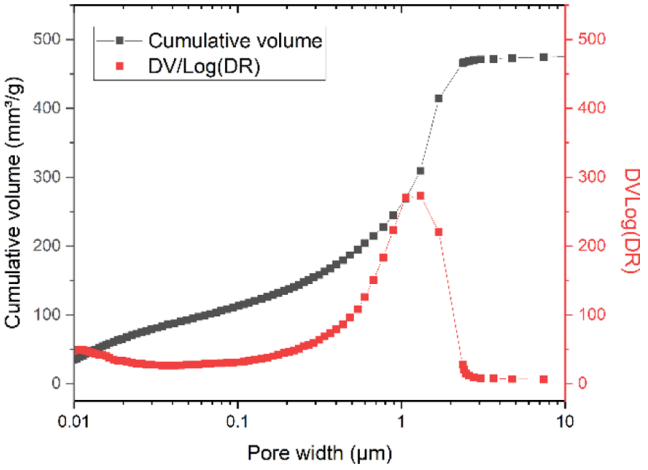

Figure 8. Cumulative pore volume and pore size distribution as derived from the mercury intrusion measurement on the activated carbon/silicate glue-printed composite.

CO_2 Adsorption. The cyclic CO_2 sorption capacity of the composite monoliths was evaluated and compared to the activated carbon powder by TGA. In the first step, the sample was degassed at 120 °C in a N_2 flow for 3 h. After regeneration and cooling to room temperature, 9.1% CO_2 was added to the sample chamber, and the weight increase over time was evaluated (cycle 1). Following this adsorption step, desorption of the CO_2 gas is induced by flowing pure N_2 for 3 h through the sample chamber at room temperature. This cycle is repeated three times in total to evaluate the regenerability and performance of the sorbent with only a N_2-flush (no heating). The comparison of the activated carbon powder and the activated carbon/glue composite in crushed and structured form is shown in Figure 9. As observed, the CO_2 capacity of the activated carbon powder is stable over the different cycles; the material can be fully regenerated by N_2 purging without an increase in temperature during the desorption step. A total CO_2 uptake capacity at 9.1% CO_2 of 0.28 mmol/g is observed for the activated carbon powder. On contrary to the activated carbon powder, the composite shows a significant decrease in sorption capacity throughout the different cycles. This decrease can be attributed to the different adsorption mechanism of the 3D-printed composite material. The pure activated carbon powder displays excellent regenerability without heating the material, which can be explained by physisorption of CO_2 on the large specific surface area. For the monolith adsorbent, on the other hand, the significant drop in adsorption capacity throughout the ad- and desorption cycles combined with the slightly decreased specific surface area, indicating the occurrence of a much stronger bond between the adsorbed CO_2 and the surface of the material. The amount of available adsorption sites decreases significantly throughout the different cycles, leading to an overall reduction of the total adsorption capacity. Comparing the capacities of the powdered composite to the structured monolith, there is a negligible impact of the

https://doi.org/10.1021/acsomega.2c07074
ACS Omega 2023, 8, 4116−4126

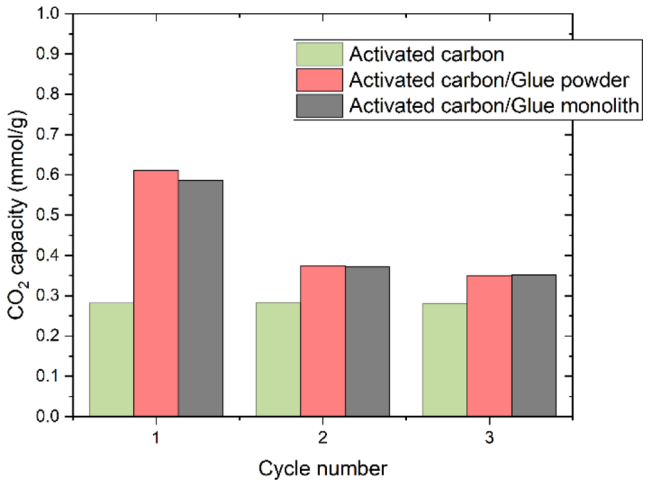

Figure 9. Comparison of the cyclic CO_2 sorption capacity at 9.1% CO_2 in N_2 (25 °C, 1 bar), analyzed by TGA. The sample is degassed at 120 °C prior to the first cycle and subsequently regenerated at room temperature in the following cycles.

shaping process on the CO_2 uptake capacity. No significant decrease in capacity is observed comparing the composite in crushed powder form with the composite in structured monolith form throughout the three cycles, which indicates a high accessibility of the activated carbon powder and the potassium silicate glue.

In order to fully regenerate the composite sorbent, two different desorption temperatures were evaluated (100 and 150 °C) (see Figure 10). In the first step, a similar degassing

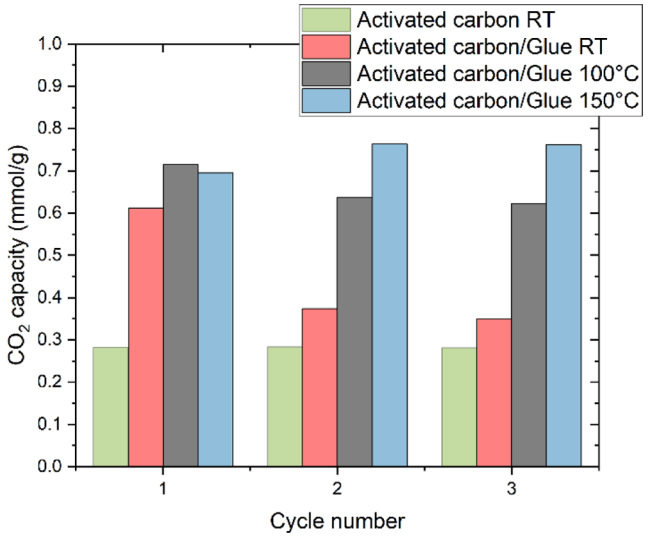

Figure 10. Effect of desorption temperature on the cyclic CO_2 capacity of the activated carbon/glue composite at N_2-9.1% CO_2, analyzed by TGA.

procedure at 120 °C was applied as described in the previous paragraph. Adsorption was then carried out by using a 9.1% CO_2 in N_2 stream, resulting in the total CO_2 sorption capacity displayed at cycle number 1. A sorption capacity between 0.60 and 0.70 mmol/g is shown for all three samples after cycle 1, indicating the reproducibility of the composite material.

The first desorption step is then induced by increasing the temperature from room temperature up to 100 or 150 °C under N_2 flow. While a regeneration at room temperature significantly reduced the working capacity of the sorbent material by 40% (0.61 to 0.37 mmol/g), regeneration at 100 °C only decreased the working capacity by 11% (0.7 to 0.62 mmol/g). Furthermore, the sorption capacity of the material regenerated at 150 °C induced a significant increase of the CO_2 uptake by 10% (0.69 to 0.76 mmol/g). In comparison with the reduction of the CO_2 uptake after desorption at room temperature, regenerating at higher temperatures clearly induces a significant increase in the CO_2 uptake, indicating the recovery of the active sites. In comparison with the activated carbon powder, this results in a CO_2 uptake that is almost tripled (0.28 vs 0.76 mmol/g).

Using the optimized desorption procedure, the CO_2 uptake capacity was also evaluated at elevated adsorption temperatures, as shown in Figure S3 in the Supporting Information. A significant decrease of the uptake capacity is observed when increasing the temperature, going from 0.761 mmol/g at 25 °C to 0.576 and 0.372 mmol/g for 50 and 75 °C, respectively. This trend indicates the importance of the flue gas temperature when using an activated carbon composite for CO_2 adsorption out of flue gases.

CO_2-Adsorption Mechanism. The TGA results indicate a change in the sorption mechanism when adding the silicate glue to the activated carbon powder. While porosimetry measurements show the decreased specific surface area and micropore volume of the composite material, significantly higher sorption capacities were observed even after multiple cycles with room temperature regeneration. Additionally, TGA experiments show that the active sites require higher temperatures in order to achieve full regeneration. Both observations indicate that the composite material adsorbs CO_2 by a combination of physisorption in the remaining pores of the activated carbon and chemisorption.

As indicated in the literature,[43,44] this chemisorption process is most likely the (partial) conversion of potassium bicarbonate ($KHCO_3$) to potassium carbonate (K_2CO_3) or intermediate hydrated forms. The incomplete regeneration at room temperature indicates that this regeneration is not sufficient to recover all chemisorption sites. Interestingly, the addition of this glue also increases the working capacity, even after regeneration at room temperature by N_2 flushing. The full CO_2-adsorption mechanism is shown in eqs 1−5, with the first reaction already occurring during curing after shaping.

First of all, the aqueous silicate solution (indicated by the characterization of the pure glue) will transition to a carbonate, which will function as the active sorption species, and silica which will act as a binder and provide mechanical strength to the printed composite.

Transition from silicate to carbonate

$$K_2SiO_3 + 2CO_2 + H_2O \leftrightarrow 2KHCO_3 + SiO_2 \quad (1)$$

During the pretreatment of the carbonate (through the partial mechanism and/or full mechanism, depending on the presence of water and the utilized temperature), CO_2 is released, with the formation of potassium carbonate hydrate or anhydrous potassium carbonate.

Desorption reaction

$$\text{Partial: } 2KHCO_3 + 0.5H_2O \leftrightarrow K_2CO_3 \cdot 1.5H_2O + CO_2 \quad (2)$$

$$\text{Full: } 2KHCO_3 \leftrightarrow K_2CO_3 + H_2O + CO_2 \quad (3)$$

https://doi.org/10.1021/acsomega.2c07074
ACS Omega 2023, 8, 4116−4126

This pretreated 3D-printed monolith then adsorbs CO_2 with the formation of potassium bicarbonate through both reverse reactions:

Adsorption reaction

$$\text{Partial: } K_2CO_3 \cdot 1.5H_2O + CO_2 \leftrightarrow 2KHCO_3 + 0.5\,H_2O \quad (4)$$

$$\text{Full: } K_2CO_3 + CO_2 + H_2O \leftrightarrow 2KHCO_3 \quad (5)$$

To confirm the described mechanism including the conversion of potassium bicarbonate ($KHCO_3$) to potassium carbonate (K_2CO_3) at higher desorption temperatures, an in situ XRD study was performed, where the temperature of the composite sample was increased stepwise up to 150 °C. Figure 11 shows the diffraction pattern of the activated carbon/silicate glue composite. The composite was measured in crushed form at room temperature and subsequently heated in situ to 150 °C in the air atmosphere. Several XRD scans were performed during heating to evaluate the transformation of the characteristic peaks. At room temperature, three characteristic peaks can be observed at 28.18, 35.05, and 36.55°, indicating the presence of $KHCO_3$. A clear reduction in peak intensities is observed with increasing temperature, confirming the conversion of $KHCO_3$ to K_2CO_3. Complete conversion of $KHCO_3$ is observed after heating to 150 °C.

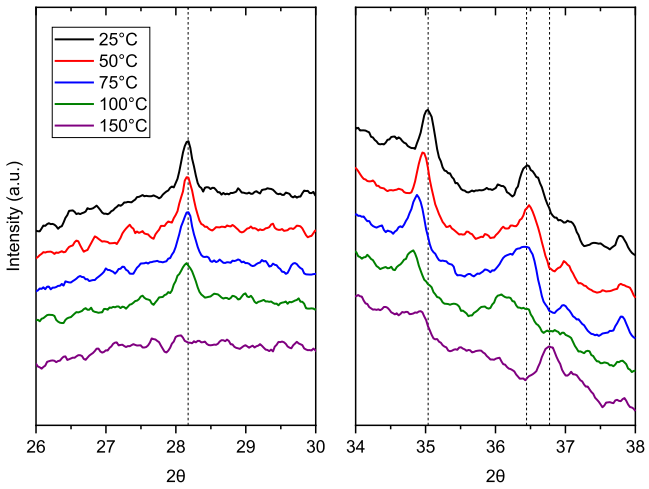

Figure 11. Temperature-controlled XRD spectrum of the AC/glue composite to investigate the transition of $KHCO_3$ to K_2CO_3 at elevated temperatures.

This mechanism, confirmed by XRD, also explains why the incorporation of additional potassium silicate molecules does not result in a capacity increase (Figure 3). As described with other carbonation reactions,[45,46] the adsorption of CO_2 by the potassium atoms creates an external layer of potassium carbonate, limiting the diffusion to and accessibility of internal potassium atoms. Therefore, the particle size and the specific surface area of the activated carbon largely influence the availability of the potassium atoms and the overall adsorption capacity.

These in situ XRD observations, coupled with the increased working capacities as displayed in the earlier TGA-looping experiments, show the large potential of the silicate glue as an active low-temperature binder for the creation of strong monolithic activated carbon structures, suitable for a low-temperature and energy-efficient regeneration.

Joule Heating. First, the electrical resistivity was measured on the activated carbon powder as well as fibers of the composite using a two-probe method. The resistivity is an important property since it determines the efficiency and homogeneity of the heating process. Low electrical resistivity could result in inhomogeneous heating due to high contact resistances while increased electrical resistivities typically lead to the need of elevated voltages to achieve conductivity throughout the structure. The electrical resistivity of the composite was measured on several fiber lengths (0.5−1.0 cm), resulting in a value of 0.014 Ω m, while the activated carbon powder showed a resistivity of 0.0021 Ω m. This value clearly indicates the increase in electrical resistivity caused by the addition of the potassium silicate binder. To evaluate the effect of the potassium silicate binder on the homogeneity of the heat development throughout the activated carbon composite, cyclic Joule heating experiments were performed on the structured adsorbent (see Figure 1 in the Experimental Section for a picture of the utilized setup). Figure 12a shows an infrared picture of the heated monolith during the first temperature cycle. The temperature distribution of the structured composite adsorbent was very homogeneous, as observed in Figure 12a,b. The lowest temperature of the monolith was located at the bottom left corner of the IR image in Figure 12a, which is the location of the pressurized air nozzle applying active cooling to the structured sample (see Figure 1). Furthermore, a slight decrease in temperature was observed at the vertical sides of the structured monolith due to natural convection. To evaluate the temperature distribution across the two electrodes, the minimum, maximum, and average temperatures on a line perpendicular to the electrodes were measured over time, as depicted in Figure 12b. Fast and homogeneous heating was observed, with average heating times of 54 °C/min during the application of the current. Moreover, an increased heating rate was observed at the lower temperatures, being 110 °C/min from 30 to 40 °C and 90 °C/min from 40 to 50 °C. The maximum temperature difference across the line throughout the structure was equal to 18.4 °C at an average temperature of 82 °C but decreases to 11.5 °C at the maximum temperature.

Graphs of temperature rates and temperature differences between maximum and minimum temperature, as well as a heat map over time are included in the Supporting Information.

With this preliminary experiment, the homogeneity of the heat development as well as the applicability to use the material for CO_2 separation by ESA has been shown. However, a more detailed study of the performance of the composite material in an ESA process for biogas upgrading was described previously by Verougstraete et al.[36]

CONCLUSIONS

In this work, structured activated carbon sorbents suitable for Joule heating and electrical swing adsorption were developed using the 3D micro-extrusion technology by using potassium silicate as a low-temperature binder. A paste optimization was performed to achieve a balance between the printability, mechanical strength of the sorbent after printing and a maximized CO_2 sorption capacity. Several monolithic/multichannel type structures were developed and characterized in terms of total pore volume, pore size distribution, and the resulting CO_2 uptake. As observed using thermogravimetric analysis with 9.1% CO_2 in N_2, the use of the silicate binder

https://doi.org/10.1021/acsomega.2c07074
ACS Omega 2023, 8, 4116−4126

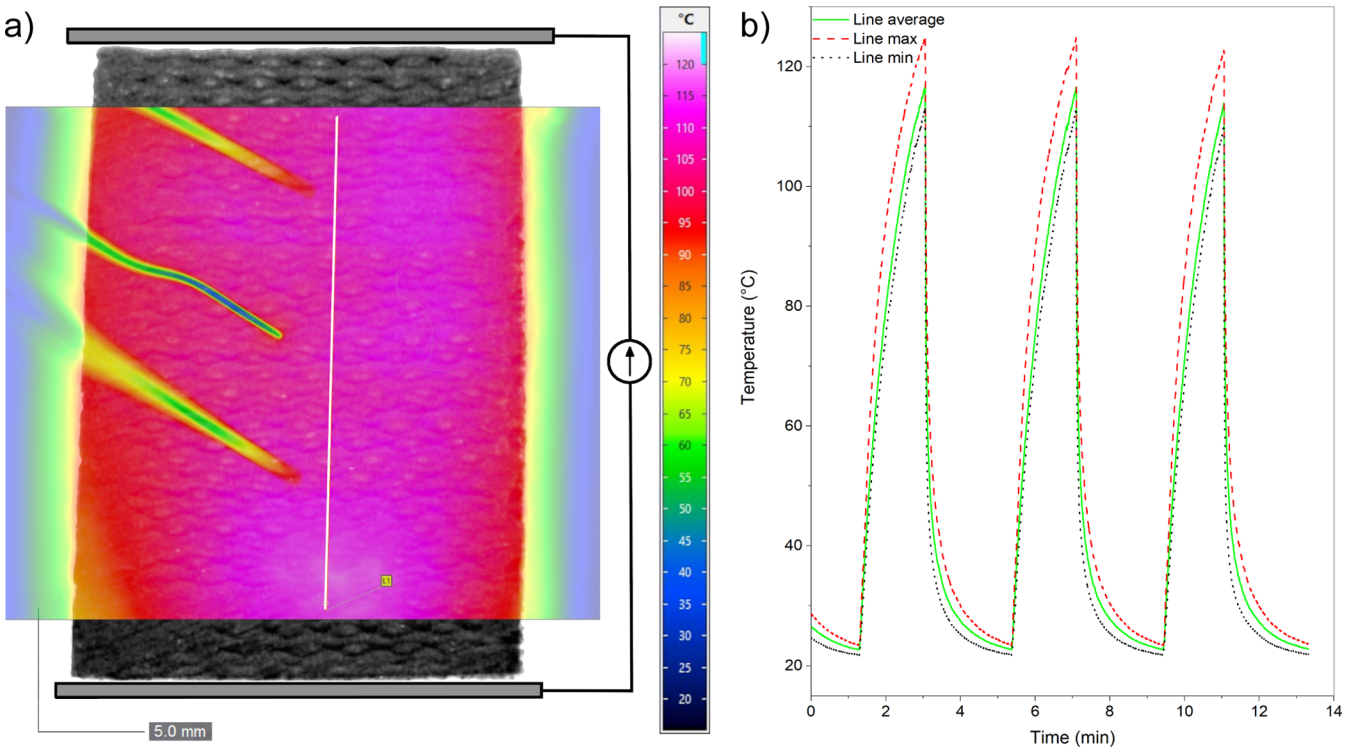

Figure 12. (a) Infrared overlay on microscopy image of the side of the monolith (color scale bar between 15 °C and 125 °C, length scale bar 5 mm). Aluminum electrode locations are schematically drawn on the image. (b) Temperature profile (minimum, average, and maximum) of the line indicated on the infrared overlay during 3 J heating cycles.

doubled the working capacity of the 3D-printed activated carbon sorbent after a regeneration step of 120 °C. This working capacity dropped after regeneration at room temperature using N_2-purging but still exceeded the CO_2 uptake of the original activated carbon powder by 25%. By increasing the regeneration temperature up to 150 °C, an improved working capacity of the composite material up to 0.76 mmol/g was observed after several cycles, almost tripling the working capacity of the original activated carbon powder (0.28 mmol/g). An in situ XRD study confirmed the proposed mechanism, including a combination of physisorption in the remaining activated carbon micropores and chemisorption, resulting in the formation of potassium bicarbonates. The cyclic Joule heating experiments indicated the possibility of fast and homogeneous heating cycles (an average heating rate of 54 °C/min from 23.5 to 125 °C), with a maximum temperature difference of 18.4 °C between the two electrodes during heating. These results show the large potential of the silicate glue as an active low-temperature binder for creating strong monolithic activated carbon structures, suitable for low-temperature and energy-efficient regeneration using Joule heating.

■ ASSOCIATED CONTENT

Supporting Information

The Supporting Information is available free of charge at https://pubs.acs.org/doi/10.1021/acsomega.2c07074.

Temperature rates and temperature differences during Joule heating, as well as a heat map over time (PDF)

■ AUTHOR INFORMATION

Corresponding Author

Ben Sutens − *Sustainable Materials Department, Flemish Institute for Technological Research—VITO, 2400 Mol, Belgium;* orcid.org/0000-0003-4556-9498; Phone: +32 14 33 54 62; Email: ben.sutens@vito.be

Authors

Yoran De Vos − *Sustainable Materials Department, Flemish Institute for Technological Research—VITO, 2400 Mol, Belgium*

Brieuc Verougstraete − *Department of Chemical Engineering, Vrije Universiteit Brussel, 1050 Brussels, Belgium*

Joeri F. M. Denayer − *Department of Chemical Engineering, Vrije Universiteit Brussel, 1050 Brussels, Belgium;* orcid.org/0000-0001-5587-5136

Marleen Rombouts − *Sustainable Materials Department, Flemish Institute for Technological Research—VITO, 2400 Mol, Belgium;* orcid.org/0000-0003-3916-1971

Complete contact information is available at: https://pubs.acs.org/10.1021/acsomega.2c07074

Author Contributions

All authors have given approval to the final version of the manuscript.

Funding

The authors are grateful to FWO Vlaanderen for financial support for the CATCO2RE project (S004118N).

Notes

The authors declare no competing financial interest.

https://doi.org/10.1021/acsomega.2c07074
ACS Omega 2023, 8, 4116−4126

■ ACKNOWLEDGMENTS

The authors want to express their thank to R. Kemps, M. Mertens, and A. De Wilde for their significant contribution by performing the SEM, XRD, and porosity/TGA measurements, respectively.

■ REFERENCES

(1) Younas, M.; Sohail, M.; Leong, L. K.; Bashir, M. J.; Sumathi, S. Feasibility of CO2 Adsorption by Solid Adsorbents: A Review on Low-Temperature Systems. *Int. J. Environ. Sci. Technol.* **2016**, *13*, 1839−1860.

(2) Cai, Y.; Wang, W.; Li, L.; Wang, Z.; Wang, S.; Ding, H.; Zhang, Z.; Sun, L.; Wang, W. Effective Capture of Carbon Dioxide Using Hydrated Sodium Carbonate Powders. *Materials* **2018**, *11*, 183.

(3) MacDowell, N.; Florin, N.; Buchard, A.; Hallett, J.; Galindo, A.; Jackson, G.; Adjiman, C. S.; Williams, C. K.; Shah, N.; Fennell, P. An Overview of CO2 Capture Technologies. *Energy Environ. Sci.* **2010**, *3*, 1645−1669.

(4) Rezaei, F.; Webley, P. Structured Adsorbents in Gas Separation Processes. *Sep. Purif. Technol.* **2010**, *70*, 243−256.

(5) Raganati, F.; Chirone, R.; Ammendola, P. CO2 Capture by Temperature Swing Adsorption: Working Capacity As Affected by Temperature and CO2 Partial Pressure. *Ind. Eng. Chem. Res.* **2020**, *59*, 3593−3605.

(6) Ben-Mansour, R.; Qasem, N. A. A. An Efficient Temperature Swing Adsorption (TSA) Process for Separating CO2 from CO2/N2 Mixture Using Mg-MOF-74. *Energy Convers. Manage.* **2018**, *156*, 10−24.

(7) Rainone, F.; D'Agostino, O.; Erto, A.; Balsamo, M.; Lancia, A. Biogas Upgrading by Adsorption onto Activated Carbon and Carbon Molecular Sieves: Experimental and Modelling Study in Binary CO2/CH4 Mixture. *J. Environ. Chem. Eng.* **2021**, *9*, 106256.

(8) Morales-Ospino, R.; Santiago, R. G.; Siqueira, R. M.; de Azevedo, D. C. S.; Bastos-Neto, M. Assessment of CO2 Desorption from 13X Zeolite for a Prospective TSA Process. *Adsorption* **2020**, *26*, 813−824.

(9) An, H.; Feng, B.; Su, S. CO2 Capture by Electrothermal Swing Adsorption with Activated Carbon Fibre Materials. *Int. J. Greenhouse Gas Control* **2011**, *5*, 16−25.

(10) Grande, C. A.; Ribeiro, R. P. L.; Oliveira, E. L. G.; Rodrigues, A. E. Electric Swing Adsorption as Emerging CO2 Capture Technique. *Energy Procedia* **2009**, *1*, 1219−1225.

(11) Sullivan, P. D.; Rood, M. J.; Grevillot, G.; Wander, J. D.; Hay, K. J. Activated Carbon Fiber Cloth Electrothermal Swing Adsorption System. *Environ. Sci. Technol.* **2004**, *38*, 4865−4877.

(12) Middelkoop, V.; Coenen, K.; Schalck, J.; Van Sint Annaland, M.; Gallucci, F. 3D Printed versus Spherical Adsorbents for Gas Sweetening. *Chem. Eng. J.* **2019**, *357*, 309−319.

(13) Ruthven, D. M.; Thaeron, C. Performance of a Parallel Passage Adsorbent Contactor. *Sep. Purif. Technol.* **1997**, *12*, 43−60.

(14) Querejeta, N.; Plaza, M. G.; Rubiera, F.; Pevida, C.; Avery, T.; Tennisson, S. R. Carbon Monoliths in Adsorption-Based Post-Combustion CO2 Capture. *Energy Procedia* **2017**, *114*, 2341−2352.

(15) Thakkar, H.; Eastman, S.; Hajari, A.; Rownaghi, A. A.; Knox, J. C.; Rezaei, F. 3D-Printed Zeolite Monoliths for CO2 Removal from Enclosed Environments. *ACS Appl. Mater. Interfaces* **2016**, *8*, 27753−27761.

(16) Lefevere, J.; Claessens, B.; Mullens, S.; Baron, G.; Cousin-Saint-Remi, J.; Denayer, J. F. M. 3D-Printed Zeolitic Imidazolate Framework Structures for Adsorptive Separations. *ACS Appl. Nano Mater.* **2019**, *2*, 4991−4999.

(17) Regufe, M. J.; Ferreira, A. F. P.; Loureiro, J. M.; Rodrigues, A.; Ribeiro, A. M. Electrical Conductive 3D-Printed Monolith Adsorbent for CO2 Capture. *Microporous Mesoporous Mater.* **2019**, *278*, 403−413.

(18) Sun, Y.; Wang, Y.; Zhang, Y.; Zhou, Y.; Zhou, L. CO2 Sorption in Activated Carbon in the Presence of Water. *Chem. Phys. Lett.* **2007**, *437*, 14−16.

(19) Silva, J. A. C.; Schumann, K.; Rodrigues, A. E. Sorption and Kinetics of CO2 and CH4 in Binderless Beads of 13X Zeolite. *Microporous Mesoporous Mater.* **2012**, *158*, 219−228.

(20) Indira, V.; Abhitha, K. A Review on Polymer Based Adsorbents for CO2 Capture. *IOP Conf. Ser.: Mater. Sci. Eng.* **2021**, *1114*, 012081.

(21) Song, K. S.; Fritz, P. W.; Coskun, A. Porous Organic Polymers for CO2 Capture, Separation and Conversion. *Chem. Soc. Rev.* **2022**, *51*, 9831.

(22) Landaverde-Alvarado, C.; Morris, A. J.; Martin, S. M. Gas Sorption and Kinetics of CO2 Sorption and Transport in a Polymorphic Microporous MOF with Open Zn(II) Coordination Sites. *J. CO2 Util.* **2017**, *19*, 40−48.

(23) Santos, K. M. C.; Santos, R. J. O.; De Araújo Alves, M. M.; De Conto, J. F.; Borges, G. R.; Dariva, C.; Egues, S. M.; Santana, C. C.; Franceschi, E. Effect of High Pressure CO2 Sorption on the Stability of Metalorganic Framework MOF-177 at Different Temperatures. *J. Solid State Chem.* **2019**, *269*, 320−327.

(24) Lyu, H.; Li, H.; Hanikel, N.; Wang, K.; Yaghi, O. M. Covalent Organic Frameworks for Carbon Dioxide Capture from Air. *J. Am. Chem. Soc.* **2022**, *144*, 12989−12995.

(25) Zhu, Y.; Zhu, D.; Yan, Q.; Gao, G.; Xu, J.; Liu, Y.; Alahakoon, S. B.; Rahman, M. M.; Ajayan, P. M.; Egap, E.; Verduzco, R. Metal Oxide Catalysts for the Synthesis of Covalent Organic Frameworks and One-Step Preparation of Covalent Organic Framework-Based Composites. *Chem. Mater.* **2021**, *33*, 6158−6165.

(26) Jing, J.-y.; Li, T.-y.; Zhang, X.-w.; Wang, S.-d.; Feng, J.; Turmel, W. A.; Li, W.-y. Enhanced CO2 Sorption Performance of CaO/Ca3Al2O6 Sorbents and Its Sintering-Resistance Mechanism. *Appl. Energy* **2017**, *199*, 225−233.

(27) Park, S. W.; Sung, D. H.; Choi, B. S.; Oh, K. J.; Moon, K. H. Sorption of Carbon Dioxide onto Sodium Carbonate. *Sep. Sci. Technol.* **2006**, *41*, 2665−2684.

(28) Serna-Guerrero, R.; Da'na, E.; Sayari, A. New Insights into the Interactions of CO2 with Amine-Functionalized Silica. *Ind. Eng. Chem. Res.* **2008**, *47*, 9406−9412.

(29) Darunte, L. A.; Walton, K. S.; Sholl, D. S.; Jones, C. W. CO2 Capture via Adsorption in Amine-Functionalized Sorbents. *Curr. Opin. Chem. Eng.* **2016**, *12*, 82−90.

(30) Guo, Y.; Zhao, C.; Li, C.; Wu, Y. CO2 Sorption and Reaction Kinetic Performance of K2CO3/AC in Low Temperature and CO2 Concentration. *Chem. Eng. J.* **2015**, *260*, 596−604.

(31) Zhao, C.; Chen, X.; Zhao, C. CO2 Absorption Using Dry Potassium-Based Sorbents with Different Supports. *Energy Fuels* **2009**, *23*, 4683−4687.

(32) Hayashi, H.; Taniuchi, J.; Furuyashiki, N.; Sugiyama, S.; Hirano, S.; Shigemoto, N.; Nonaka, T. Efficient Recovery of Carbon Dioxide from Flue Gases of Coal-Fired Power Plants by Cyclic Fixed-Bed Operations over K_2CO_3-on-Carbon. *Ind. Eng. Chem. Res.* **1998**, *37*, 185−191.

(33) Thakkar, H.; Eastman, S.; Al-Naddaf, Q.; Rownaghi, A. A.; Rezaei, F. 3D-Printed Metal-Organic Framework Monoliths for Gas Adsorption Processes. *ACS Appl. Mater. Interfaces* **2017**, *9*, 35908−35916.

(34) Lawson, S.; Al-Naddaf, Q.; Newport, K.; Rownaghi, A.; Rezaei, F. Assessment of CO2/CH4 Separation Performance of 3D-Printed Carbon Monoliths in Pressure Swing Adsorption. *Ind. Eng. Chem. Res.* **2021**, *60*, 16445−16456.

(35) Couck, S.; Cousin-Saint-Remi, J.; Van der Perre, S.; Baron, G. v.; Minas, C.; Ruch, P.; Denayer, J. F. M. 3D-Printed SAPO-34 Monoliths for Gas Separation. *Microporous Mesoporous Mater.* **2018**, *255*, 185−191.

(36) Verougstraete, B.; Schoukens, M.; Sutens, B.; Vanden Haute, N.; De Vos, Y.; Rombouts, M.; Denayer, J. F. M. Electrical Swing Adsorption on 3D-Printed Activated Carbon Monoliths for CO2 Capture from Biogas. *Sep. Purif. Technol.* **2022**, *299*, 121660.

(37) Rodríguez, M. T.; Pfeiffer, H. Sodium Metasilicate (Na2SiO3): A Thermo-Kinetic Analysis of Its CO2 Chemical Sorption. *Thermochim. Acta* **2008**, *473*, 92−95.

https://doi.org/10.1021/acsomega.2c07074
ACS Omega 2023, 8, 4116−4126

(38) Rodríguez-Mosqueda, R.; Pfeiffer, H. High CO2 Capture in Sodium Metasilicate (Na2SiO3) at Low Temperatures (30−60°C) through the CO2−H2O Chemisorption Process. *J. Phys. Chem. C* **2013**, *117*, 13452−13461.
(39) Yan, X.; Li, Y.; Ma, X.; Zhao, J.; Wang, Z. Performance of Li4SiO4 Material for CO2 Capture: A Review. *Int. J. Mol. Sci.* **2019**, *20*, 928.
(40) Essaki, K.; Nakagawa, K.; Kato, M.; Uemoto, H. Co2 Absorption by Lithium Silicate at Room Temperature. *J. Chem. Eng. Jpn.* **2004**, *37*, 772−777.
(41) Sanna, A.; Ramli, I.; Maroto-Valer, M. M. Novel Na-Silicates CO2 Sorbents from Fly Ash. *Energy Procedia* **2014**, *63*, 739−744.
(42) Thommes, M.; Kaneko, K.; Neimark, A. v.; Olivier, J. P.; Rodriguez-Reinoso, F.; Rouquerol, J.; Sing, K. S. W. Physisorption of Gases, with Special Reference to the Evaluation of Surface Area and Pore Size Distribution (IUPAC Technical Report). *Pure Appl. Chem.* **2015**, *87*, 1051−1069.
(43) Borhani, T. N. G.; Azarpour, A.; Akbari, V.; Wan Alwi, S. R.; Manan, Z. A. CO2 Capture with Potassium Carbonate Solutions: A State-of-the-Art Review. *Int. J. Greenhouse Gas Control* **2015**, *41*, 142−162.
(44) Isa, F.; Zabiri, H.; Ng, N. K. S.; Shariff, A. M. Purification of CO2 Removal via Promoted Potassium Carbonate: A Review on Modelling & Simulation Techniques. *Int. J. Greenhouse Gas Control* **2018**, *76*, 236−265.
(45) Sanna, A.; Ramli, I.; Maroto-Valer, M. M. Novel Na-Silicates CO2 Sorbents from Fly Ash. *Energy Procedia* **2014**, *63*, 739−744.
(46) Rodríguez, M. T.; Pfeiffer, H. Sodium Metasilicate (Na2SiO3): A Thermo-Kinetic Analysis of Its CO2 Chemical Sorption. *Thermochim. Acta* **2008**, *473*, 92−95.

https://doi.org/10.1021/acsomega.2c07074
ACS Omega 2023, 8, 4116−4126